

Enhancement of Bose glass phase in presence of artificial gauge field

Sukla Pal,¹ Rukmani Bai,^{1,2} Soumik Bandyopadhyay,^{1,2} K. Suthar,¹ and D. Angom¹

¹*Physical Research Laboratory, Ahmedabad - 380009, Gujarat, India*

²*Indian Institute of Technology Gandhinagar, Palaj, Gandhinagar - 382355, Gujarat, India*

We study the effect of diagonal disorder on zero and finite temperature phase diagrams of two dimensional Bose Hubbard model. Employing single site and cluster Gutzwiller mean field theory we incorporate the effect of disorder which results in the formation of Bose glass phase. This inhibits direct transition from Mott insulator to superfluid phase. The use of cluster Gutzwiller mean field improves the correlation and there is enlargement of the Bose glass phase region. Similar enlargement is observed on introducing artificial gauge field. More importantly, to relate with the experimental realization we include finite temperature effects, and this leads to melting of Bose glass as well as the Mott insulator phase.

I. INTRODUCTION

The observation of superfluid (SF) to Mott insulator (MI) transition in an optical lattice [1], well described by Bose-Hubbard model (BHM), have opened a new paradigm to explore the physics of quantum many-body systems. Optical lattices are clean and highly controllable, in contrast, the condensed matter systems of interest are never devoid of impurities. Thus, some of the fundamental questions in experimental condensed matter physics are related to quantum phase transitions in the presence of finite disorder. In optical lattices which are excellent proxies of condensed matter systems, the equivalent system is BHM with static disorder [2, 3]. The presence of disorder constrains the evolution of a quantum system in the Hilbert space and gives rise to new quantum glassy phases like Bose glass (BG) [4] and disorder enhanced mechanisms like Anderson localizations [5–8] in strongly correlated systems.

In the case of BHM, random off set energy (disorder) and repulsive onsite interaction have opposing effects on bosons in optical lattices. The role of these two competing effects is the key to explore the glassy behavior of the BG phase in disordered Bose Hubbard model (DBHM). The early theoretical investigations [3] showed that there is no MI-SF transition in presence of diagonal disorder as the BG phase always occurs in between the two phases. The theorem of inclusion [9, 10] agrees well with this prediction while identifying BG phase as a Griffith's phase containing the rare regions in a gapped MI to gapless SF transition. In these rare-regions, the energy gap of adding another boson to the system vanishes and thus can be identified as SF islands.

Experimentally, DBHM can be realized by the addition of speckle type of disorder [11–13], or by the generation of incommensurate multichromatic lattice [14, 15]. Indirect measurements on SF-BG transition have been reported in 1D [16] and 3D [17] systems through transport and coherence measurements. While the detection of the same transition in 3D was recently performed by quenching the disorder strength [18]. In 2D, the observation of center of mass dynamics [19] has been theoretically proposed as a method to detect the BG phase in a parabolic confining potential. On the other hand there is a proposal [20] to measure radius of atomic cloud to detect BG phase. There are also other proposals to detect BG phase based on the idea of replica of disorder distribution [21]

and replica symmetry breaking [22]. In spite of these various proposals and progresses towards the realization of a Bose glass, the clear and strong experimental evidence of BG phase is still missing. However, the local measurement is very crucial in detecting the BG phase since it is composed of rare regions or SF islands. Experimentally, this requires high resolution optical imaging schemes such as quantum gas microscope [23], and have been proposed as an experimental tool to detect BG phases [24].

The theoretical studies of DBHM have been done with diverse techniques: mean field [25], projected Gutzwiller method [4], site independent and multisite mean-field method [26, 27], stochastic mean field [28], quantum Monte Carlo [29–31], density matrix renormalisation group (DMRG) [32, 33] for 1D system and numerous others [34–38]. In all the cases the introduction of disorder leads to the emergence of BG phase. This new phase is characterized by finite compressibility and non zero superfluid stiffness. In the present work, we study 2D DBHM both at zero and at finite temperatures. Here, it must be emphasized that theoretical investigations of DBHM are usually at zero temperatures, but the experimental measurements for obvious thermodynamical reasons are always at finite temperatures. This gap is addressed in the present work by examining the consequent effects of finite temperatures to BG phase. One key finding is the presence of normal fluid (NF) phase at finite temperatures and melting of Bose glass phase. The latter is consistent with the experimental findings reported in ref. [24]. We also study the effect of artificial gauge field on the BG phase, and find that the region of BG phase in the phase diagram is enhanced. For these studies we use single site Gutzwiller and cluster Gutzwiller mean field theories.

This paper is organized as follows in the Section. II we give an account of the single site and cluster Gutzwiller mean field theories. This is then followed by a description of the artificial gauge field and observable measures to distinguish different phases in Section. III and IV. Then, in Section V we provide detailed description of the results obtained from our studies and discuss our observations. And, we then, conclude.

II. MODEL AND GUTZWILLER MEAN FIELD THEORY

The DBHM for a square lattice with nearest neighbour hopping is defined by the Hamiltonian

$$\hat{H} = - \sum_{p,q} \left[J_x \left(\hat{b}_{p+1,q}^\dagger \hat{b}_{p,q} + \text{H.c.} \right) + J_y \left(\hat{b}_{p,q+1}^\dagger \hat{b}_{p,q} + \text{H.c.} \right) \right] + \sum_{p,q} \hat{n}_{p,q} \left[\frac{U}{2} (\hat{n}_{p,q} - 1) - \tilde{\mu}_{p,q} \right], \quad (1)$$

where p (q) is the lattice index along x (y) axis, $\hat{b}_{p,q}^\dagger$ ($\hat{b}_{p,q}$) are the creation (annihilation) operators for a boson at the (p, q) lattice site, $\hat{n}_{p,q}$ is the boson density operator; J_x (J_y) is the hopping strength between two NN sites along x (y) axis, $U > 0$ is the on-site inter-atomic interaction strength, and $\tilde{\mu}_{p,q} = \mu - \epsilon_{p,q}$ is the local chemical potential. The disorder is introduced through the random energy offset $\epsilon_{p,q}$ which is a uniformly distributed independent random numbers $r_j \in [-D, D]$ Depending on the ratio of J and U the above Hamiltonian can describe three possible phases of the system— MI, BG and SF [3]. In the strong on-site interaction limit ($J/U \rightarrow 0$) the system is either in the MI-phase (gapped phase), or in BG phase. Whereas the system is in SF phase when the tunneling overcomes repulsive interaction.

A. Zero temperature Gutzwiller mean-field theory

In the present work we employ Gutzwiller mean-field theory to compute the properties of the DBHM. In this subsection we describe two variants of Gutzwiller mean field theory. First is the single site Gutzwiller mean-field (SGMF) method, where the lattice sites are correlated through a scalar mean field ϕ and cannot describe entangled states like quantum Hall state. And, the second is the cluster Gutzwiller mean field (CGMF) method, which incorporates the correlation within a cluster of neighbouring lattice sites exactly and inter-cluster correlation through ϕ . Larger cluster captures better correlation effects at the cost of higher computation.

1. SGMF method

In the SGMF method, $\hat{b}_{p,q}$ ($\hat{b}_{p,q}^\dagger$) at a particular lattice site (p, q) is decomposed into mean field $\phi_{p,q}$ ($\phi_{p,q}^*$) and fluctuation $\delta\hat{b}_{p,q}$ ($\delta\hat{b}_{p,q}^\dagger$) parts as

$$\hat{b}_{p,q} = \phi_{p,q} + \delta\hat{b}_{p,q}, \quad (2a)$$

$$\hat{b}_{p,q}^\dagger = \phi_{p,q}^* + \delta\hat{b}_{p,q}^\dagger \quad (2b)$$

where, $\phi_{p,q} = \langle \hat{b}_{p,q} \rangle$, and $\phi_{p,q}^* = \langle \hat{b}_{p,q}^\dagger \rangle$ are the mean field and its complex conjugate, respectively. The expectations are defined with respect to the ground state of the system. Employing this decomposition, the Hamiltonian in Eq. (1) is reduced

to the SGMF Hamiltonian

$$\hat{H}^{\text{MF}} = \sum_{p,q} \left\{ - J_x \left[\left(\hat{b}_{p+1,q}^\dagger \phi_{p,q} + \phi_{p+1,q}^* \hat{b}_{p,q} - \phi_{p+1,q}^* \phi_{p,q} \right) + \text{H.c.} \right] - J_y \left[\left(\hat{b}_{p,q+1}^\dagger \phi_{p,q} + \phi_{p,q+1}^* \hat{b}_{p,q} - \phi_{p,q+1}^* \phi_{p,q} \right) + \text{H.c.} \right] + \left[\frac{U}{2} \hat{n}_{p,q} (\hat{n}_{p,q} - 1) - \tilde{\mu}_{p,q} \hat{n}_{p,q} \right] \right\}, \quad (3)$$

where terms up to linear in fluctuation operators are considered and those quadratic in fluctuation operators are neglected. The total Hamiltonian in the above expression can be rewritten as $\hat{H}^{\text{MF}} = \sum_{p,q} \hat{H}_{p,q}^{\text{MF}}$, where $\hat{H}_{p,q}^{\text{MF}}$ is the single site mean field Hamiltonian. The mean field $\phi_{p,q}$ can be identified as the SF order parameter which defines the MI to BG phase-transition in DBHM. Thus, $\phi_{p,q}$ is zero, when the system is in MI phase, and finite in BG as well as SF phase.

To compute the ground state of the system the Hamiltonian matrix of $\hat{H}_{p,q}^{\text{MF}}$ can be diagonalized for each site separately. And, then the ground state of the system is direct product of the single site ground states $|\psi\rangle_{p,q}$. Using the Gutzwiller approximation, the groundstate of the system is

$$|\Psi_{\text{GW}}\rangle = \prod_{p,q} |\psi\rangle_{p,q} = \prod_{p,q} \sum_{n=0}^{N_b} c_n^{(pq)} |n\rangle_{p,q}, \quad (4)$$

where N_b is the maximum allowed occupation number basis (Fock space basis), and $c_n^{(pq)}$ are the co-efficients of the occupation number state $|n\rangle$ at the lattice site (p, q) . From $|\Psi_{\text{GW}}\rangle$ we can calculate $\phi_{p,q}$, the SF order parameter, as

$$\phi_{p,q} = \langle \Psi_{\text{GW}} | \hat{b}_{p,q} | \Psi_{\text{GW}} \rangle = \sum_{n=0}^{N_b} \sqrt{n} c_{n-1}^{(pq)*} c_n^{(pq)}. \quad (5)$$

From the above expression it is evident that $\phi_{p,q}$ is zero in the MI phase as only one occupation number state $|n\rangle$ contributes to $|\psi\rangle_{p,q}$ and hence only one $c_n^{(pq)}$ has nonzero value. Similarly, the occupancy and number fluctuation at a lattice site are

$$\langle \hat{n}_{p,q} \rangle = \sum_{n=0}^{N_b} |c_n^{(pq)}|^2 n_{p,q}, \quad (6)$$

$$\delta n_{p,q} = \sqrt{\langle \hat{n}_{p,q}^2 \rangle - \langle \hat{n}_{p,q} \rangle^2} \quad (7)$$

In the MI phase $\delta n_{p,q}$ is zero, which makes MI phase incoherent. In the BG and SF phase $\delta n_{p,q}$ has nonzero value, but the values of $\delta n_{p,q}$ in the BG phase is very small which arises due to the presence of SF islands in the BG phase. The nonzero and relatively large $\delta n_{p,q}$ in the SF phase indicates strong phase coherence. Thus $\delta n_{p,q}$ can also be considered as the order parameter for MI-BG phase transition.

2. CGMF method

In the CGMF method, to incorporate the hopping term exactly and hence improve the correlation effects, the total lat-

tice considered is partitioned into clusters. That is, for an optical lattice of dimension $K \times L$, we can separate it into W clusters (C) of size $M \times N$, that is $W = (K \times L)/(M \times N)$. Thus, the case of CGMF with $M = N = 1$ is equivalent to SGMF. In CGMF, the kinetic energy or the hopping term is decomposed into two types. First is the intra-cluster or hopping within the lattice sites in a cluster, and second is the inter-cluster which is between neighbouring lattice sites which lie on the boundary of different clusters. The details of the present implementation of the CGMF method is reported in ref. [39]. and the Hamiltonian of a single cluster is

$$\begin{aligned} \hat{H}_C = & - \sum_{p,q \in C} ' \left[J_x \hat{b}_{p+1,q}^\dagger \hat{b}_{p,q} + J_y \hat{b}_{p,q+1}^\dagger \hat{b}_{p,q} + \text{H.c.} \right] \\ & - \sum_{p,q \in \delta C} \left[J_x (\phi_{p+1,q}^c)^* \hat{b}_{p,q} + J_y (\phi_{p,q+1}^c)^* \hat{b}_{p,q} + \text{H.c.} \right] \\ & + \sum_{p,q \in C} \left[\frac{U}{2} \hat{n}_{p,q} (\hat{n}_{p,q} - 1) - \tilde{\mu}_{p,q} \hat{n}_{p,q} \right] \end{aligned} \quad (8)$$

where $(\phi_{p,q}^c)^* = \sum_{p',q' \notin C} \langle b_{p',q'} \rangle$ is the SF order parameter at the lattice site which lies at the boundary of neighbouring cluster. The prime in the summation of the first term is to indicate that the $(p+1, q)$ and $(p, q+1)$ lattice points are also within the cluster. And, in the second term δC denotes the lattice sites at the boundary of the cluster. The matrix element of \hat{H}_C is defined in terms of the cluster basis states

$$|\Phi_c\rangle_\ell = \prod_{q=0}^{M-1} \prod_{p=0}^{N-1} |n_p^q\rangle, \quad (9)$$

where $|n_p^q\rangle$ is the occupation number basis at the (p, q) lattice site, and $\ell \equiv \{n_0^1, n_1^1, \dots, n_{M-1}^1, n_0^2, n_1^2, \dots, n_{M-1}^2, \dots, n_{M-1}^{N-1}\}$ is the index quantum number to identify the cluster state. After diagonalizing the Hamiltonian, we can get the ground state of the cluster as

$$|\Psi_c\rangle = \sum_\ell C_\ell |\Phi_c\rangle_\ell. \quad (10)$$

The ground state of the entire $K \times L$ lattice, like in SGMF, is the direct product of the cluster ground states

$$|\Psi_{\text{GW}}^c\rangle = \prod_k |\Psi_c\rangle_k \quad (11)$$

where, k is the cluster index and varies from 1 to $W = (K \times L)/(M \times N)$. The SF order parameter ϕ is computed similar to Eq. (5) as

$$\phi_{p,q} = \langle \Psi_{\text{GW}}^c | \hat{b}_{p,q} | \Psi_{\text{GW}}^c \rangle. \quad (12)$$

With respect to cluster basis, the average occupancy and number fluctuation of lattice sites in the k th cluster are

$$\langle \hat{n} \rangle_k = \frac{\sum_{p,q \in C} \langle \hat{n}_{p,q} \rangle_k}{MN} \quad (13)$$

$$(\delta n)_k = \sqrt{\langle \hat{n}^2 \rangle_k - \langle \hat{n} \rangle_k^2}. \quad (14)$$

For the entire lattice, the average density can be defined as the mean of the average occupancy of the clusters.

B. Finite temperature Gutzwiller mean field theory

To incorporate finite temperature effects we require the entire set of eigenvalues and eigenfunctions obtained from the diagonalization of the mean field Hamiltonian. So, in the case of SGMF we use all the single site eigenvectors $|\psi\rangle_{p,q}^k$ and corresponding eigenvalues $E_{p,q}^k$ to define the single site partition function

$$Z = \sum_{k=1}^{N_b} e^{-\beta E_k}, \quad (15)$$

where $\beta = 1/k_B T$, T being the temperature of the system. Since the energy E_k is scaled with respect to U , T is in units of U/k_B or in other words in the rest of the paper temperature is defined in terms of the dimensionless unit $k_B T/U$. In a similar way, for the CGMF we can define the cluster partition function in terms of the eigenfunctions $|\Psi\rangle_c^k$ and the corresponding eigenvalues. Using the above description, the thermal average of the SF order parameter at the (p, q) lattice site is

$$\langle \phi_{p,q} \rangle = \frac{1}{Z} \sum_{k=0}^{N_b} \langle \psi | \hat{b}_{p,q} e^{-\beta E_k} | \psi \rangle_c^k, \quad (16)$$

where $\langle \dots \rangle$ is used to represent thermal averaging. Similarly, the occupancy or the density can be computed as

$$\langle \langle \hat{n}_{p,q} \rangle \rangle = \frac{1}{Z} \sum_{k=0}^{N_b} \langle \psi | \hat{n}_{p,q} e^{-\beta E_k} | \psi \rangle_c^k, \quad (17)$$

where, following the notations in Eq. (7) and (14), the additional $\langle \dots \rangle$ represents thermal averaging. Once we obtain $\langle \langle \hat{n}_{p,q} \rangle \rangle$, the average density or occupancy is $\langle \rho \rangle = \langle n \rangle = \sum_{p,q} \langle \langle \hat{n}_{p,q} \rangle \rangle / (K \times L)$. Then, like defined earlier, the number fluctuation is

$$\langle \delta n \rangle_{p,q} = \sqrt{\langle \hat{n}^2 \rangle - \langle \hat{n} \rangle^2}. \quad (18)$$

A new feature of considering finite temperature effects is, it is possible to have vanishing $\langle \phi_{p,q} \rangle$ but with non-integer $\langle \langle \hat{n}_{p,q} \rangle \rangle$. This heralds a new phase in the phase diagram and is referred to as the normal fluid (NF). Thus, at finite temperatures SF order parameter can act as the order parameter for the NF-BG transition and MI-NF transition as well as for NF-BG transition. Compared to the NF phase, the MI on the other hand has vanishing $\langle \phi_{p,q} \rangle$ and integer $\langle \langle \hat{n}_{p,q} \rangle \rangle$. So, with vanishing $\langle \phi_{p,q} \rangle$ the change from integer value to non-integer $\langle \langle \hat{n}_{p,q} \rangle \rangle$ can be identified MI-NF transition.

III. ARTIFICIAL GAUGE FIELD

Artificial gauge fields [40–42] engineered through optical fields can create synthetic magnetic fields for charge neutral ultracold atoms in optical lattices. This generates an equivalent of Lorentz force for these atoms, and optical lattice is,

then, endowed with properties analogous to the quantum Hall system. Such a system is an excellent model system to study the physics of strongly correlated states like quantum Hall states and their properties. The same logic also applies to the DBHM. In the Hamiltonian description, the presence of an artificial gauge field induces a complex hopping parameter $J \rightarrow J \exp(i\Phi)$ and accordingly single site Hamiltonian in Eq. (3) is modified to

$$\begin{aligned} \hat{H}^{\text{MF}} = \sum_{p,q} \left\{ -J_x e^{i\Phi} \left[\left(\hat{b}_{p+1,q}^\dagger \phi_{p,q} + \phi_{p+1,q}^* \hat{b}_{p,q} \right. \right. \right. \\ \left. \left. - \phi_{p+1,q}^* \phi_{p,q} \right) + \text{H.c.} \right] - J_y \left[\left(\hat{b}_{p,q+1}^\dagger \phi_{p,q} \right. \right. \\ \left. \left. + \phi_{p,q+1}^* \hat{b}_{p,q} - \phi_{p,q-1}^* \phi_{p,q} \right) + \text{H.c.} \right] \\ \left. + \left[\frac{U}{2} \hat{n}_{p,q} (\hat{n}_{p,q} - 1) - \tilde{\mu}_{p,q} \hat{n}_{p,q} \right] \right\}, \quad (19) \end{aligned}$$

where, Φ is the phase an atom acquires when it traverses around a unit cell or plaquette, the artificial gauge field is considered in the Landau gauge and the phase for hopping along x direction arises via the Peierls substitution [43, 44]. The artificial gauge field, then, creates a staggered synthetic magnetic flux [45] along y direction. The phase can also be defined in terms of the α , the flux quanta per plaquette, through the relation $\Phi = 2\pi\alpha q$, and the flux is restricted in the domain $0 \leq \alpha \leq 1/2$. In present work, we examine the property of bosons in presence of artificial gauge field while experiencing random local chemical potential. Although, the effect of artificial gauge field on BHM is quite well studied, the same is not true of DBHM.

IV. CHARACTERIZATION OF STATES

Each of the low temperature phases supported by DBHM has special properties and this leads to unique combinations of order parameters as signatures of each phase. The values of these order parameters also determine the phase boundaries. In Table. I, we list the order parameters corresponding to each phases.

A. Superfluid stiffness and compressibility

Phase coherence is a characteristic property of the SF phase, and it is absent in the other phases (MI, NF and BG) supported by DBHM. Thus in the SF phase it requires finite amount of energy to alter the phase coherence, or in other words, it acquires stiffness towards phase change. This property is referred to as the superfluid stiffness ρ_s , and hence plays an important role in determining the phase boundary between BG and SF phase. To compute ρ_s , a twisted boundary condition (TBC) is imposed on the state. If the TBC is applied along the x direction, the hopping term in the DBHM is

transformed as

$$J_x (b_{p+1,q}^\dagger b_{p,q} + \text{H.c.}) \rightarrow J_x (b_{p+1,q}^\dagger b_{p,q} e^{i2\pi\varphi/L} + \text{H.c.}), \quad (20)$$

where, φ is the phase shift or twist applied to the periodic boundary condition, L is the size of the lattice along x direction, and $2\pi\varphi/L$ is phase shift of an atom when it hops between nearest neighbours. Accordingly, ρ_s is computed employing the following expression [33]

$$\rho_s = \frac{L}{8\pi^2} \frac{\partial^2 E_0}{\partial \phi^2} \Big|_{\phi=0}. \quad (21)$$

The SF phase is a compressible state as δn is finite. However, MI phase and strongly correlated phase like quantum Hall states are incompressible. Thus, the compressibility κ is a property of the system which can be employed a diagnostic to support the phases determined through the order parameters. By definition, κ is given by

$$\kappa = \frac{\partial \langle \hat{n} \rangle}{\partial \mu}. \quad (22)$$

That is, κ is the sensitivity of n to the change of μ .

B. Edwards-Anderson order parameter

For a disordered system the natural and hence, more appropriate order parameter is the Edwards-Anderson order parameter (EAOP). It can distinguish the Griffith's phase by its non zero value and can describe the effect of disorder better than other properties like ρ_s , κ , structure factor, etc. In the studies with mean field theory, EAOP was first introduced to detect the non trivial breaking of ergodicity. Since then various type of EAOP have been proposed in literature [21, 22, 46, 47]. In our study we consider the EAOP of the following form [22]

$$q_{\text{EA}} = \overline{\langle \hat{n}_{p,q} \rangle^2} - \overline{\langle \hat{n}_{p,q} \rangle}^2, \quad (23)$$

where, $n_{p,q}$ is the number of atoms at the (p, q) lattice site. The above expression involves two types of averages: $\langle \dots \rangle$ represents thermal; and $\overline{\dots}$ indicates average over disorder distribution. For the $\langle \dots \rangle$ we consider all the excited states, and for the $\overline{\dots}$ we take the average of 50 realizations of disorder distribution. From the definition, as MI phase identified by integer values of $\langle \hat{n}_{p,q} \rangle$ EAOP is zero. In the SF phase $\langle \hat{n}_{p,q} \rangle$ is non-integer and $\delta n_{p,q}$ is finite, hence EAOP finite but small $O(10^{-2})$. But EAOP is finite in the BG phase due to correlation between number density and disorder. Thus using EAOP the BG phase is distinguishable from other phases, MI, SF and NF, present in the system. In zero temperature limit we define EAOP as

$$q_{\text{EA}}|_{(t=0)} = \overline{\hat{n}_{p,q}^2} - \overline{\hat{n}_{p,q}}^2, \quad (24)$$

where, we consider $n_{p,q}$ only for the ground state.

Quantum phase	Order parameter
Superfluid (SF)	$q_{EA} = 0, \rho_s > 0, \kappa > 0, \phi \neq 0$
Mott insulator (MI)	$q_{EA} = 0, \rho_s = 0, \kappa = 0, \phi = 0$
Bose glass (BG)	$q_{EA} > 0, \rho_s = 0, \kappa > 0, \phi \neq 0$
Normal fluid (NF)	$q_{EA} > 0, \rho_s = 0, \kappa > 0, \phi = 0$

TABLE I. Classification of quantum phases and the order parameters supported by DBHM at zero and at finite temperatures.

V. RESULTS AND DISCUSSIONS

To compute the ground state of the system and determine the phase diagram, we scale the parameters of the DBHM Hamiltonian with respect to the interaction strength U . So, the relevant parameters of the model are J/U , μ/U and D/U . We, then, determine the phase diagram of the DBHM in the $J/U - \mu/U$ plane for different values of D/U , and one unique feature of the model is the emergence of the BG phase. The local glassy nature of the BG phase leads to very different properties from the incompressible and gapped MI phase, and compressible and gapless SF phase. Thus as mentioned earlier, one of the key issues in the study of DBHM is to identify appropriate order parameters to distinguish different phases. And, in particular, to determine the BG phase without ambiguity based on its local properties. To construct the phase diagram, we consider a 12×12 square lattice superimposed with a homogeneous disorder distribution. An example of the disorder distribution employed in our computation for $D/U = 1.2$ is shown in Fig. 1. The distribution is such that every site has a random offset energy that lies in the domain $[-D/2, D/2]$.

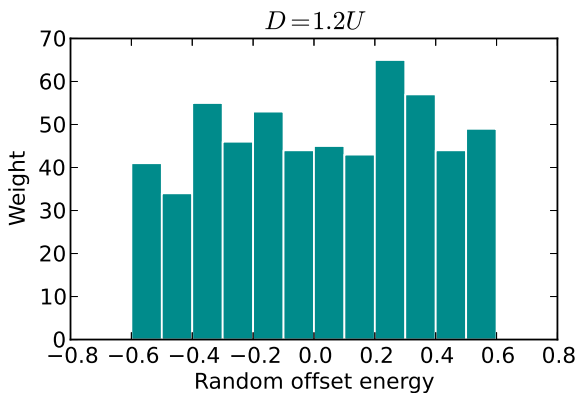


FIG. 1. Sample distribution of random offset energies $\epsilon_{p,q}$. The trend is suggestive of random but homogeneous distribution and since the $D/U = 1.2$, the local chemical potential variation is from -0.6 to 0.6 .

In DBHM, depending on the magnitude of D/U , the phase diagrams can be classified into three broad categories. First, at low disorder strength $D/U \leq 0.1$, BG phase emerge in the phase diagram. Second, at moderate disorder strengths $0.2 \leq D/U \leq 1$, the domain of BG phase is enhanced. This is the most important regime to explore the physics of BG phase. The distinctive features in this range consist of (a) shrinking

of Mott region (b) enhancement of BG phase and (c) BG-SF transition occurs at higher J/U . Finally, at very high disorder strengths $D/U > 1$, MI phase disappears and DBHM supports only two phases BG and SF.

A. Zero temperature results

Our zero temperature studies of DBHM, as mentioned earlier, is in two domains: without artificial gauge field ($\alpha = 0$), and finite artificial gauge field ($\alpha \neq 0$). For the latter we consider a range of α , and in particular, focus on the results from $\alpha = 1/4$. The order parameter at each lattice site $\phi_{p,q}$ for the two cases are shown in Fig. 2. In the figure Fig. 2(a)-(c) show the spatial distribution of $\phi_{p,q}$ for MI, BG and SF phases, respectively, with a disorder strength of 0.6 and $\alpha = 0$ at $J/U = 0.015$ for different values of μ/U . And, the Fig. 2(d)-(f) correspond to same disorder strength and distribution, but non-zero artificial gauge field with $\alpha = 1/4$. The BG phase in Fig. 2(b) shows the SF islands immersed in the MI region ($\phi_{p,q} = 0$). Whereas the SF phase in Fig. 2(c) has $\phi_{p,q}$ varying randomly over a homogeneous background value. With non-zero artificial gauge field, the BG phase as shown in Fig. 2(e) exhibits reduction of the SF islands. In addition, the SF phase in Fig. 2(f) shows the formation of SF islands in MI background and loses its homogeneity due to vortex formation [40]. Further more, as the artificial gauge field tends to localize the atoms and there is a delay in the percolation as a function of J/U [10, 48]. This has direct impact on the DBHM phase diagram.

1. Phase diagram with $\alpha = 0$

The phase diagrams for the case of $D/U = 0, 0.2, 0.6$ and 1.2 with $\alpha = 0$ and obtained from the SGMF method are shown in Fig. 2(g)-(j). As mentioned earlier, the phase diagrams at different values of D/U have distinctive features. With $D/U = 0$, the phase diagram as shown in Fig. 2(g) consists of only two phases MI and SF. With non-zero D/U BG emerges in the phase diagram, and as shown in Fig. 2(h) for 0.2 the domain of the MI phase shrinks and an envelope of BG phase emerges around the MI lobes. From Fig. 2(h), it is clear that the presence of BG phase is most prominent in the regions which lie between the MI lobes. These are the domains where there are large density fluctuations and small disorder is sufficient to render the bosons itinerant to create islands of SF phase. This, then, leads to the formation of BG phase. When D/U is increased to 0.6, as shown in Fig. 2(i), the MI lobes continue to shrink and area of the BG phase is further enlarged. At sufficiently high disorder strength, $D = 1.2U$, the MI phase disappears and phase diagram Fig. 2(j) is composed of only SF and BG phases.

To determine the MI-BG phase boundary we consider number fluctuation (δn) as the properties which distinguishes the two phases. In the MI phase δn is zero for $D/U = 0$, however, for $D/U \neq 0$ it is non-zero but small due to the disorder. We set $\delta n < 10^{-6}$ as the criterion to identify the MI phase

in our computations. On the other hand, to define the BG-SF boundary, we compute the superfluid stiffness (ρ_s). In BG phase as the SF phase exists as islands the phase coherence is limited to these, so the ρ_s small, and we consider $\rho_s < 10^{-2}$ as the threshold to distinguish the BG from SF phase. In the SF phase as there is phase coherence throughout the system ρ_s is large and it is $O(1)$.

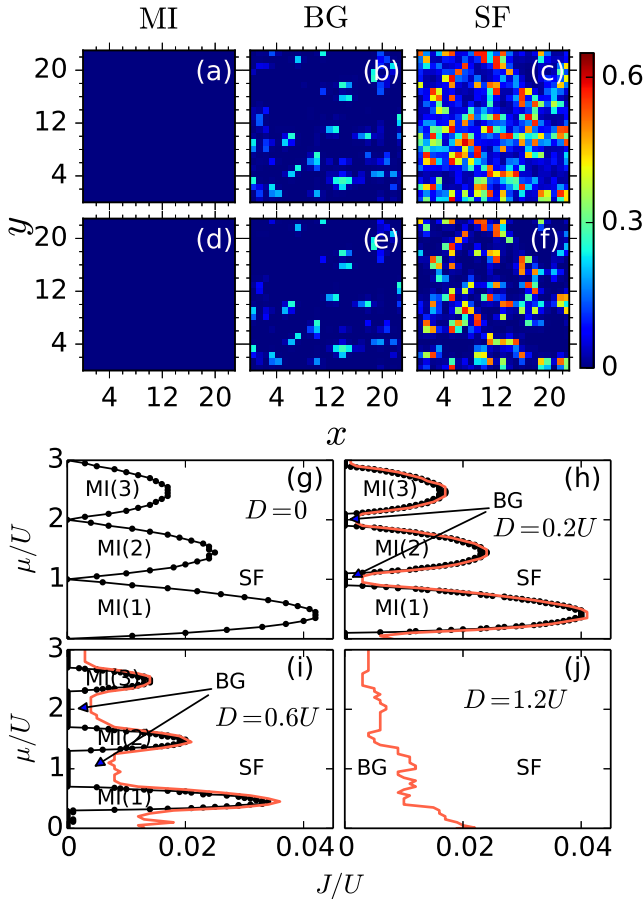


FIG. 2. Order parameter ϕ of DBHM at zero temperature for $J/U = 0.015$ choosing $D/U = 0.06$ (a)-(c) without and (d)-(f) with ($\alpha = 1/4$) artificial gauge field. (a) & (d) MI phase with $\mu/U = 0.5$; (b) & (e) BG phase with $\mu/U = 0.1$; and (c) & (f) SF phase with $\mu/U = 1.0$. (g)-(j) equilibrium phase diagram of DBHM using SGMF method at zero temperature in absence of artificial gauge field ($\alpha = 0$) for disorder strengths $D/U = 0.0, 0.2, 0.6$ and 1.2 , respectively.

There is an improvement in the phase diagram, which is apparent from the enlarged MI lobes, when the phase diagram is computed using CGMF. In particular, we consider 2×2 cluster and the phase diagrams so obtained are shown in Fig. 3. The overall structure of the phase diagram is qualitatively similar to the SGMF case. However, there are few quantitative changes. For comparison, consider the case of $D/U = 0.6$, based on our results and as visible in Fig. 2(c) and Fig. 3(b), there are three important difference due to better correlation effects encapsulated in the CGMF method. First, the tip of the Mott lobe 1 extends upto 0.035 while it was

0.032 with SGMF. This is due to the better correlation effects in the CGMF, the Mott lobe in SGMF is smaller as lower correlation favours SF over MI phase. Second, at $\mu/U \simeq 0$, the SF-BG transition occurs at $J/U \approx 0.022$, which in the case of SGMF is at $J/U \approx 0.016$. This is due to the association of BG phase with islands of SF phase, and CGMF captures the phase correlations in these islands. The SGMF, on the other hand, tends to favour long range phase correlations through the ϕ coupling between the lattices sites. And, finally, around the tip of the Mott lobes, the area of BG phase increases in CGMF method.

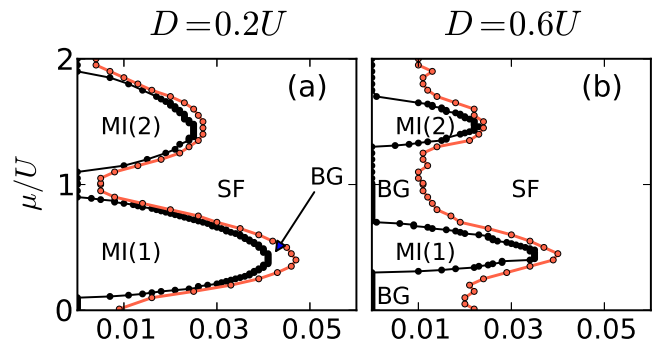


FIG. 3. Equilibrium phase diagram of DBHM using CGMF method with cluster size 2×2 at zero temperature in absence of artificial gauge field for disorder strength (a) $D/U = 0.2$, and (b) $D/U = 0.6$

2. Phase diagram with $\alpha = 1/4$

The introduction of artificial gauge field, in the present work, leads to a synthetic magnetic field in the DBHM. The synthetic magnetic field produce an analogue Lorentz force for the bosons, which localizes the bosons and suppresses their itinerant property. This manifests as a larger MI lobe in the presence of artificial gauge field. However, at a smaller scale the combined effect of disorder and artificial gauge field favours formation of islands of SF phase. This synergy, then, creates a larger domain of BG phase in the phase diagram. In terms of identifying the phase boundaries, unlike in the $\alpha = 0$ where ρ_s has linear dependence on J/U in the SF domain, ρ_s cannot be use as it exhibits no dependence on J/U . The two possible causes of this are: the twisted boundary condition required to compute ρ_s modifies the magnetic unit cell associated with the chosen value of α ; and with $\alpha \neq 0$ the SF phase contains vortices which reduce the SF phase coherence. So, we use EAOP as the order parameter to distinguish BG phase from the MI and SF phases. The general trend is that EAOP is close to zero in MI and SF phase and finite in BG phase. For consistency we compute EAOP for the case of $\alpha = 0$ with SGMF and is shown in Fig. 4, where EAOP is shown as a function of μ/U and J/U . From the figure, the presence of the BG phase between different MI lobes is discernible from the finite values of EAOP and it is consistent with the phase diagram determined from ρ_s shown in Fig. 2. We can define sharp MI-BG and SF-BG boundaries in the phase diagram by defining a threshold value of EAOP between the Mott lobes,

however, this is non-trivial for the patina of BG phase present at the tip of Mott lobes.

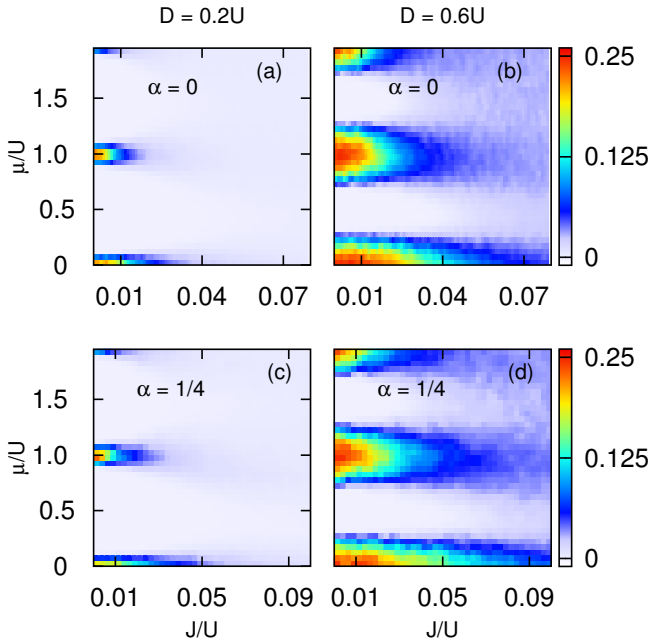


FIG. 4. EAOP parameter q_{EA} at zero temperature as a function of μ/U and J/U in absence of artificial gauge field with disorder strength (a) $D/U = 0.2$, and (b) $D/U = 0.6$. With artificial gauge field are shown for (c) $D/U = 0.2$, and (d) $D/U = 0.6$.

At finite artificial gauge field with $\alpha = 1/4$ the domain of the BG phase is enhanced. This is discernible from the plot of EAOP for two disorder strengths $D/U = 0.2$ and $D/U = 0.6$ as shown in Fig. 4(c)-(d). For the case of $D/U = 0.6$ the EAOP is finite with a value of ≈ 0.2 upto $J/U \approx 0.03$. Whereas, with $\alpha = 0$ as shown in Fig. 4(b), EAOP has similar value only upto $J/U \approx 0.02$.

B. Finite temperature results

The important outcome of finite temperature is the emergence of a new phase, the normal fluid (NF) phase. In this new phase like the SF phase ρ is real and commensurate, but unlike SF ϕ is zero. So, NF phase has some features of both the MI and SF phase, but is neither of the two. The appearance of the NF at finite temperatures is also reported in the case of the canonical Bose-Hubbard model [49], and extended Bose-Hubbard model with nearest neighbour interactions [50, 51].

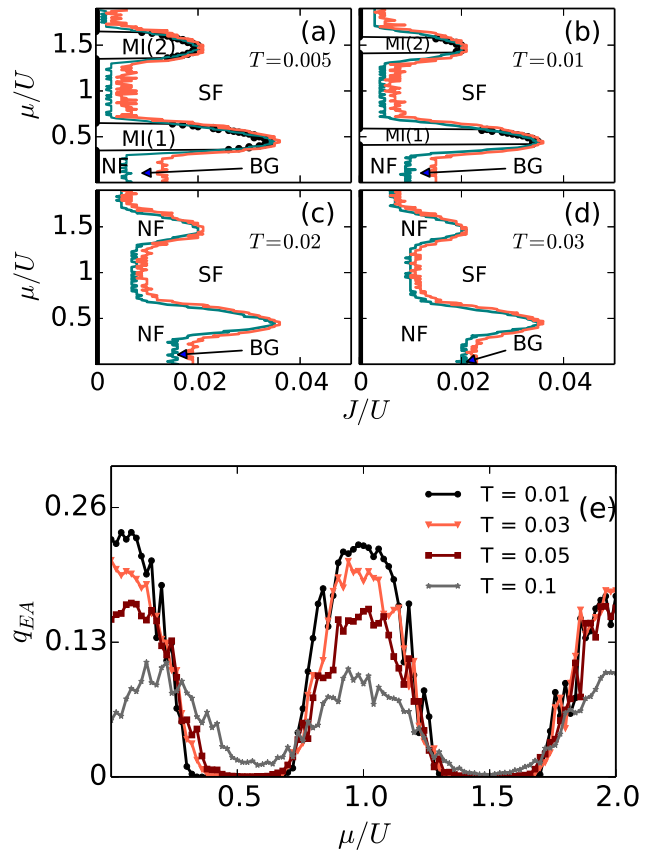


FIG. 5. Finite temperature phase diagram using SGMF method in absence of artificial gauge field for four different temperatures (a) $T = 0.005U/k_B$, (b) $T = 0.01U/k_B$, (c) $T = 0.02U/k_B$ and (d) $T = 0.03U/k_B$. Disorder strength is fixed at $D = 0.6U$ and each data in the plot is obtained by averaging over 50 different disorder distributions. (e) shows finite temperature effects on Edward-Anderson order parameter (EAOP). The magnitude of EAOP decreases with increase of temperature.

1. $\alpha = 0$

The effect of the thermal fluctuations to the EAOP, in absence of artificial gauge field ($\alpha = 0$), is shown in Fig. 5(e). The results presented in the figure correspond to $D/U = 0.6$ and each plot correspond to the average of 50 realizations of disorder distributions. With increasing temperature there is a monotonic decrease in q_{EA} , which indicates the *melting* of BG phase. Along with the BG phase the MI phase also melts, however, this is not apparent from the values of q_{EA} . The measures which can quantify melting of MI phase are the ones which identify the NF phase, and degree of melting can be inferred from the phase diagram. To illustrate this point the phase diagram of DBHM at different temperatures are shown in Fig 5. As mentioned earlier, the melting of MI phase due to thermal fluctuations was reported in previous studies [49]. On the other hand, Based on experimental studies [52], recent DMRG calculation [53] sheds some light on finite temperature effect on coherence property of DBHM phase diagram. But clear theoretical description and phase diagram incorpo-

rating finite temperature effects is available. Our present work adds to these findings the melting of BG phase due to thermal fluctuations. Here, the key point is the SF islands, which are hallmarks of BG phase, melts into NF, but the bulk SF phase does not exhibit large scale melting. This arises from the local nature of the SF islands in BG phase, which as a result are affected by the local nature of the thermal fluctuations. The bulk SF phase, on the other hand, have long range phase correlations and are more robust against local fluctuations stemming from finite temperatures.

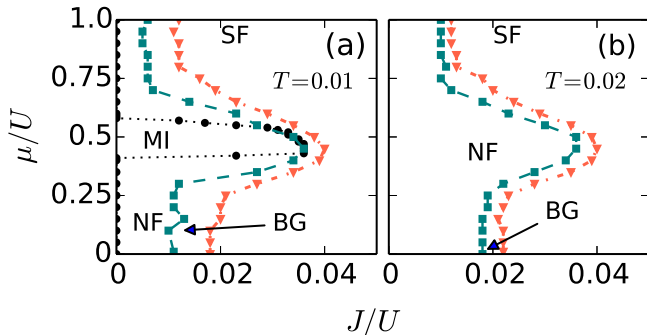


FIG. 6. Finite temperature phase diagram using CGMF for 2×2 cluster in absence of artificial gauge field for two different temperatures (a) $T = 0.01U/k_B$, (b) $T = 0.02U/k_B$; Disorder strength is fixed at $D = 0.6U$ and each data in the plot is obtained by averaging over 50 different disorder distributions.

The phase diagrams of the DBHM at different temperatures are shown in Fig. 5(a)-(d). In the plots the region within the black line is MI phase, whereas, the region bounded by the black and green lines is the NF phase, where ϕ is close to zero $\phi \leq 10^{-16}$. The BG phase lies in the region bounded by the green and orange lines, and the area right of the orange line is the SF phase. As the temperature increases, due to increased thermal fluctuation, the phase diagrams undergo several changes. First, the MI lobes shrink and at $k_B T/U = 0.02$, MI lobes disappear from the phase diagram. This is due to the melting of MI phase and conversion into NF phase. So, as discernible from the comparison of Fig. 5(a) and (b), the MI lobe with $\rho = 1$ is bounded lies in the domain $0.36 \leq \mu \leq 0.64$ at $k_B T/U = 0.005$, but it shrinks to $0.42 \leq \mu \leq 0.58$ at $k_B T/U = 0.01$. Second, the region of the BG phase is reduced with increasing temperature. The change is more prominent in the regions which were in between the MI lobes than the tips of the lobes. For example, at $\mu = 0$ which lies between the $\rho = 1$ and $\rho = 0$ MI lobes, the BG phase lies in domain $0.006 \leq J/U \leq 0.014$, $0.009 \leq J/U \leq 0.015$, $0.016 \leq J/U \leq 0.019$ and $0.02 \leq J/U \leq 0.022$ for the temperatures $k_B T/U = 0.005, 0.01, 0.02$ and 0.03 , respectively. This indicates that the NF-BG and BG-SF phase boundaries shift toward higher values of J/U . This is due to higher hopping energy required to prevail over thermal fluctuations. So that the SF phase is present as islands or homogeneous network in BG and SF phases, respectively. And, third, at finite temperatures the MI lobes are bounded from top and bottom by straight lines in the SGMF results. But, as visible from Fig. 6, the MI boundary is not a straight line with CGMF results.

This is on account of the better correlation effects in CGMF, in contrast, SGMF tends to support sharp NF-MI boundaries as a function of μ/U due to short range coupling through ϕ .

To improve the accuracy of the phase diagram by incorporating additional correlation effects, we compute the phase diagram with CGMF using 2×2 cluster, and resulting phase diagram is shown in Fig. 6. The results are for the $k_B T/U = 0.005$ and 0.02 , and for better illustration the phase diagram only upto $\mu/U = 1.0$ are shown in the figure. As to be expected the MI lobes are enlarged in the CGMF results, but the one important change with the CGMF is that the envelope of BG phase around the MI and NF phases is more pronounced. Consequent to the enlargement of MI lobes, the NF and BG phases encompasses regions with higher J/U compared with the SGMF results. In particular, at $\mu = 0$ the BG phase occurs in the domain $0.011 \leq J/U \leq 0.018$ and $0.018 \leq J/U \leq 0.022$ for the $k_B T/U = 0.01$ and $k_B T/U = 0.02$, respectively.

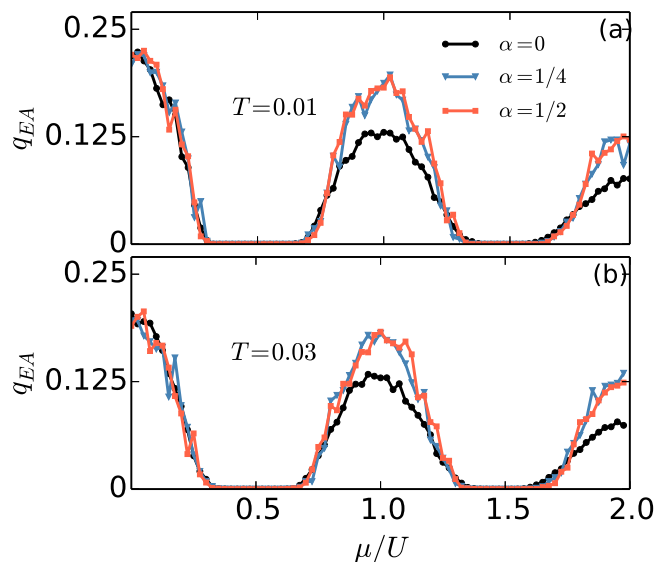


FIG. 7. EAOP at finite temperature as a function of μ/U for three different values of α at (a) $T = 0.01U/K_B$ (b) $T = 0.03U/K_B$; for fixed disorder strength $D = 0.6U$ and hopping strength $J = 0.02U$. In each subfigure EAOP are calculated for $\alpha = 0, 1/4, 1/2$ and averaged over 50 different disorder distributions.

2. $\alpha = 1/4$

The thermal fluctuations delocalise the atoms through the entire lattice, and melt MI phase and tends to reduce ϕ . Whereas, as mentioned earlier, artificial gauge field localises the atoms, and thereby enhance the MI lobes. So, these two have opposing effects on the DBHM, and the combined effect of these two physical factors on the EAOP are shown in Fig. 7. In the figure the plots of EAOP for $k_B T/U = 0.01$ and 0.03 are shown for different α as a function μ/U at $J/U = 0.02$. From the figures it is apparent that the effect of artificial gauge field is negligible in the region between the $\rho = 0$ and $\rho = 1$ Mott lobes of the phase diagram. However, in the regions be-

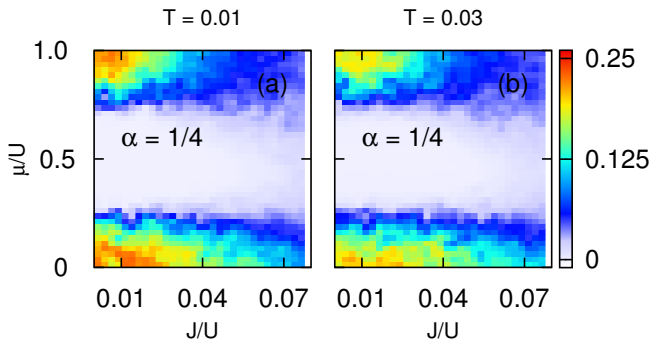


FIG. 8. EAOP at finite temperature as a function of μ/U and J/U in presence of artificial gauge field for two different values of temperature $T = 0.01U/k_B$ and $T = 0.03U/k_B$. (a)-(b) shows EAOP for $\alpha = 1/4$ and (c)-(d) corresponds to those with $\alpha = 1/6$. Disorder strength is kept fixed at $D = 0.6U$ for all the phase diagrams. In each subfigure EAOP are averaged over 50 different disorder distributions.

tween other Mott lobes there is an enhancement of the BG phase as indicated by the increase in q_{EA} . As discernible from the Fig. 7(a) the value of q_{EA} increases from 0.13 to 0.19 for the region between $\rho = 1$ and $\rho = 2$ for non-zero α at $k_B T/U = 0.01$. From the figure it is also evident that the increase in q_{EA} and hence the BG phase due to artificial gauge field is independent of its strength. This follows as there is no clear difference in the trend of q_{EA} for $\alpha = 1/4$ and $1/2$, the two corresponding curves are indistinguishable in Fig. 7. To demonstrate the effect of the combined effect of finite temperature and artificial gauge field, the phase diagram in terms of q_{EA} is shown in Fig. 8. As the figure is based on one disorder realization, the general trends of q_{EA} observable in Fig. 7 are

not apparent. However, from the figure the enlargement of the BG phase region between the MI lobes is discernible. Thus, this implies that the enhancement of the BG phase in presence of artificial gauge field is stable against thermal fluctuations.

VI. CONCLUSIONS

There is a significant difference in the phase diagram of DBHM, particularly the domain of the BG phase, obtained from the SGMF and CGMF theories. The BG phase exists in a larger domain with the CGMF theory, and forms a robust envelope around the MI phase. This is not case with SGMF, in which case the BG phase is prominent in between the MI lobes, but around the lobes. This difference is due to better description of the correlation effects in CGMF and the results are along expected lines. At finite temperatures, the thermal fluctuations leads to melting of the BG phase and formation NF phase. The emergence of the NF phase at finite temperatures necessitates using a combination order parameters and properties to identify each phase without ambiguity. Addition of artificial gauge field brings about a significant change in the phase diagram by enhancing the BG phase domain, which is observed in the trends of the EAOP without any ambiguity. This implies that such enhancements would be observable in quantum gas microscope experiments.

ACKNOWLEDGMENTS

The results presented in the paper are based on the computations using Vikram-100, the 100TFLOP HPC Cluster at Physical Research Laboratory, Ahmedabad, India.

-
- [1] M. Greiner, O. Mandel, T. Esslinger, Theodor W. Hänsch, and I. Bloch, “Quantum phase transition from a superfluid to a mott insulator in a gas of ultracold atoms,” *Nature* **415**, 39–44 (2002).
- [2] T. Giamarchi and H. J. Schulz, “Anderson localization and interactions in one-dimensional metals,” *Phys. Rev. B* **37**, 325–340 (1988).
- [3] Matthew P. A. Fisher, Peter B. Weichman, G. Grinstein, and Daniel S. Fisher, “Boson localization and the superfluid-insulator transition,” *Phys. Rev. B* **40**, 546–570 (1989).
- [4] Chien-Hung Lin, Rajdeep Sensarma, K. Sengupta, and S. Das Sarma, “Quantum dynamics of disordered bosons in an optical lattice,” *Phys. Rev. B* **86**, 214207 (2012).
- [5] P. W. Anderson, “Absence of diffusion in certain random lattices,” *Phys. Rev.* **109**, 1492–1505 (1958).
- [6] T. Schulte, S. Drenkelforth, J. Kruse, W. Ertmer, J. Arlt, K. Sacha, J. Zakrzewski, and M. Lewenstein, “Routes towards anderson-like localization of bose-einstein condensates in disordered optical lattices,” *Phys. Rev. Lett.* **95**, 170411 (2005).
- [7] Juliette Billy, Vincent Josse, Zhanchun Zuo, Alain Bernard, Ben Hambrecht, Pierre Lugan, David Clément, Laurent Sanchez-Palencia, Philippe Bouyer, and Alain Aspect, “Direct observation of anderson localization of matter waves in a controlled disorder,” *Nature* **453**, 891.
- [8] G. Roati, C. D’Errico, L. Fallani, M. Fattori, C. Fort, M. Zaccanti, G. Modugno, M. Modugno, and M. Inguscio, “Anderson localization of a non-interacting bose-einstein condensate,” *Nature* **453**, 895 (2008).
- [9] L. Pollet, N. V. Prokof’ev, B. V. Svistunov, and M. Troyer, “Absence of a direct superfluid to mott insulator transition in disordered bose systems,” *Phys. Rev. Lett.* **103**, 140402 (2009).
- [10] V. Gurarie, L. Pollet, N. V. Prokof’ev, B. V. Svistunov, and M. Troyer, “Phase diagram of the disordered bose-hubbard model,” *Phys. Rev. B* **80**, 214519 (2009).
- [11] D. Clément, A. F. Varón, M. Hugbart, J. A. Retter, P. Bouyer, L. Sanchez-Palencia, D. M. Gangardt, G. V. Shlyapnikov, and A. Aspect, “Suppression of transport of an interacting elongated bose-einstein condensate in a random potential,” *Phys. Rev. Lett.* **95**, 170409 (2005).
- [12] D. Clément, P. Bouyer, A. Aspect, and L. Sanchez-Palencia, “Density modulations in an elongated bose-einstein condensate released from a disordered potential,” *Phys. Rev. A* **77**, 033631 (2008).
- [13] M. White, M. Pasienski, D. McKay, S. Q. Zhou, D. Ceperley, and B. DeMarco, “Strongly interacting bosons in a disordered optical lattice,” *Phys. Rev. Lett.* **102**, 055301 (2009).

- [14] B. Damski, J. Zakrzewski, L. Santos, P. Zoller, and M. Lewenstein, “Atomic bose and anderson glasses in optical lattices,” *Phys. Rev. Lett.* **91**, 080403 (2003).
- [15] L. Fallani, J. E. Lye, V. Guarrera, C. Fort, and M. Inguscio, “Ultracold atoms in a disordered crystal of light: Towards a bose glass,” *Phys. Rev. Lett.* **98**, 130404 (2007).
- [16] B. Gadway, D. Pertot, J. Reeves, M. Vogt, and D. Schneble, “Glassy behavior in a binary atomic mixture,” *Phys. Rev. Lett.* **107**, 145306 (2011).
- [17] M. Pasienski, D. McKay, M. White, and B. DeMarco, “A disordered insulator in an optical lattice,” *Nature Physics* **6**, 677 (2010).
- [18] C. Meldgin, U. Ray, P. Russ, D. Chen, David M. Ceperley, and B. DeMarco, “Probing the bose glass-superfluid transition using quantum quenches of disorder,” *Nature Physics* **12**, 646 (2016).
- [19] Mi Yan, Hoi-Yin Hui, and V. W. Scarola, “Dynamics of disordered states in the bose-hubbard model with confinement,” *Phys. Rev. A* **95**, 053624 (2017).
- [20] Dominique Delande and Jakub Zakrzewski, “Compression as a tool to detect bose glass in a cold atomic gas,” *Phys. Rev. Lett.* **102**, 085301 (2009).
- [21] S. Morrison, A. Kantian, A. J. Daley, H. G. Katzgraber, M. Lewenstein, H. P. Büchler, and P. Zoller, “Physical replicas and the bose glass in cold atomic gases,” *New Journal of Physics* **10**, 073032 (2008).
- [22] S. J. Thomson and F. Krüger, “Replica symmetry breaking in the bose glass,” *EPL (Europhysics Letters)* **108**, 30002 (2014).
- [23] Waseem S. Bakr, Jonathon I. Gillen, Amy Peng, Simon Fölling, and Markus Greiner, “A quantum gas microscope for detecting single atoms in a hubbard-regime optical lattice,” *Nature* **462**, 74 (2009).
- [24] S. J. Thomson, L. S. Walker, T. L. Harte, and G. D. Bruce, “Measuring the edwards-anderson order parameter of the bose glass: A quantum gas microscope approach,” *Phys. Rev. A* **94**, 051601 (2016).
- [25] K. V. Krutitsky, A. Pelster, and R. Graham, “Mean-field phase diagram of disordered bosons in a lattice at nonzero temperature,” *New Journal of Physics* **8**, 187 (2006).
- [26] P. Buonsante, V. Penna, A. Vezzani, and P. B. Blakie, “Mean-field phase diagram of cold lattice bosons in disordered potentials,” *Phys. Rev. A* **76**, 011602 (2007).
- [27] P. Pisarski, R. M. Jones, and R. J. Gooding, “Application of a multisite mean-field theory to the disordered bose-hubbard model,” *Phys. Rev. A* **83**, 053608 (2011).
- [28] Ulf Bissbort, Ronny Thomale, and Walter Hofstetter, “Stochastic mean-field theory: Method and application to the disordered bose-hubbard model at finite temperature and speckle disorder,” *Phys. Rev. A* **81**, 063643 (2010).
- [29] H. Gimpelrein, S. Wessel, J. Schmiedmayer, and L. Santos, “Ultracold atoms in optical lattices with random on-site interactions,” *Phys. Rev. Lett.* **95**, 170401 (2005).
- [30] Ş. G. Söyler, M. Kiselev, N. V. Prokof’ev, and B. V. Svistunov, “Phase diagram of the commensurate two-dimensional disordered bose-hubbard model,” *Phys. Rev. Lett.* **107**, 185301 (2011).
- [31] Pinaki Sengupta and Stephan Haas, “Quantum glass phases in the disordered bose-hubbard model,” *Phys. Rev. Lett.* **99**, 050403 (2007).
- [32] S. Rapsch, U. Schollwöck, and W. Zwerger, “Density matrix renormalization group for disordered bosons in one dimension,” *EPL (Europhysics Letters)* **46**, 559 (1999).
- [33] M. Gerster, M. Rizzi, F. Tschirsich, P. Silvi, R. Fazio, and S. Montangero, “Superfluid density and quasi-long-range order in the one-dimensional disordered bose-hubbard model,” *New Journal of Physics* **18**, 015015 (2016).
- [34] Ramesh V. Pai, Rahul Pandit, H. R. Krishnamurthy, and S. Ramasesha, “One-dimensional disordered bosonic hubbard model: A density-matrix renormalization group study,” *Phys. Rev. Lett.* **76**, 2937–2940 (1996).
- [35] Nikolay Prokof’ev and Boris Svistunov, “Superfluid-insulator transition in commensurate disordered bosonic systems: Large-scale worm algorithm simulations,” *Phys. Rev. Lett.* **92**, 015703 (2004).
- [36] Frank Krüger, Jiansheng Wu, and Philip Phillips, “Anomalous suppression of the bose glass at commensurate fillings in the disordered bose-hubbard model,” *Phys. Rev. B* **80**, 094526 (2009).
- [37] Frank Krüger, Seungmin Hong, and Philip Phillips, “Two distinct mott-insulator to bose-glass transitions and breakdown of self-averaging in the disordered bose-hubbard model,” *Phys. Rev. B* **84**, 115118 (2011).
- [38] Juan Carrasquilla, Federico Becca, Andrea Trombettoni, and Michele Fabrizio, “Characterization of the bose-glass phase in low-dimensional lattices,” *Phys. Rev. B* **81**, 195129 (2010).
- [39] Rukmani Bai, Soumik Bandyopadhyay, Sukla Pal, K. Suthar, and D. Angom, “Bosonic quantum hall states in single layer 2d optical lattices,” [arXiv:1802.07988](https://arxiv.org/abs/1802.07988) (2018).
- [40] Y.-J. Lin, R. L. Compton, A. R. Perry, W. D. Phillips, J. V. Porto, and I. B. Spielman, “Bose-einstein condensate in a uniform light-induced vector potential,” *Phys. Rev. Lett.* **102**, 130401 (2009).
- [41] Y.-J. Lin, R. L. Compton, K. Jiménez-García, W. D. Phillips, J. V. Porto, and I. B. Spielman, “A synthetic electric force acting on neutral atoms,” *Nat Phys* **7**, 1745–2473 (2011).
- [42] J. Dalibard, F. Gerbier, Gediminas Juzeliūnas, and Patrik Öhberg, “Colloquium: Artificial gauge potentials for neutral atoms,” *Rev. Mod. Phys.* **83**, 1523–1543 (2011).
- [43] Douglas R. Hofstadter, “Energy levels and wave functions of bloch electrons in rational and irrational magnetic fields,” *Phys. Rev. B* **14**, 2239–2249 (1976).
- [44] K. Jiménez-García, L. J. LeBlanc, R. A. Williams, M. C. Beeler, A. R. Perry, and I. B. Spielman, “Peierls substitution in an engineered lattice potential,” *Phys. Rev. Lett.* **108**, 225303 (2012).
- [45] M. Aidelsburger, M. Atala, S. Nascimbéne, S. Trotzky, Y.-A. Chen, and I. Bloch, “Experimental realization of strong effective magnetic fields in an optical lattice,” *Phys. Rev. Lett.* **107**, 255301 (2011).
- [46] R. Graham and A. Pelster, “Order via nonlinearity in randomly confined bose gases,” *Int. J. Bifurcation Chaos* **19**, 2745–2753 (2009).
- [47] Tama Khellil and Axel Pelster, “Hartree-fock mean-field theory for trapped dirty bosons,” *J. Stat. Mech.* **2016**, 063301 (2016).
- [48] A. E. Niederle and H. Rieger, “Superfluid clusters, percolation and phase transitions in the disordered, two-dimensional bose-hubbard model,” *New Journal of Physics* **15**, 075029 (2013).
- [49] Fabrice Gerbier, “Boson mott insulators at finite temperatures,” *Phys. Rev. Lett.* **99**, 120405 (2007).
- [50] Kwai-Kong Ng, “Thermal phase transitions of supersolids in the extended bose-hubbard model,” *Phys. Rev. B* **82**, 184505 (2010).
- [51] Fei Lin, T. A. Maier, and V. W. Scarola, “Disordered supersolids in the extended bose-hubbard model,” *Scientific Reports* **7**, 1–10 (2017).
- [52] Chiara D’Errico, Eleonora Lucioni, Luca Tanzi, Lorenzo Gori, Guillaume Roux, Ian P. McCulloch, Thierry Giamarchi, Massimo Inguscio, and Giovanni Modugno, “Observation of a disordered bosonic insulator from weak to strong interactions,” *Phys. Rev. Lett.* **113**, 095301 (2014).

- [53] Lorenzo Gori, Thomas Barthel, Avinash Kumar, Eleonora Lucioni, Luca Tanzi, Massimo Inguscio, Giovanni Modugno, Thierry Giamarchi, Chiara D’Errico, and Guillaume Roux, “Finite-temperature effects on interacting bosonic one-dimensional systems in disordered lattices,” [Phys. Rev. A **93**, 033650 \(2016\)](#).